Electrochemical Kinetic Study of [Cp*Rh] Complexes Supported by Bis(2-pyridyl)methane Ligands

Julie A. Hopkins Leseberg, Davide Lionetti,† Victor W. Day, and James D. Blakemore*

Department of Chemistry, University of Kansas, 1567 Irving Hill Road, Lawrence, KS 66045, United States

ABSTRACT: Redox-induced reactions of organometallic complexes are ubiquitous in molecular electrochemistry and electrocatalysis research. However, detailed knowledge of the kinetic parameters associated with individual elementary steps in these reactions is often challenging to obtain, limiting understanding of the reactivity pathways that can be used to construct new catalytic cycles. Here, the kinetics of redox processes in model [Cp*Rh] complexes have been explored with substituted bis(2-pyridyl)methane (dipyridylmethane, dpma) ligands. Complementing prior work with [Cp*Rh] complexes bearing 2,2′-bipyridyl ligands, we find that the redox chemistry in these species is strongly affected by the disrupted inter-ring conjugation of dpma ligand frameworks. In particular, [Cp*Rh] complexes bearing κ^2-dpma ligands with varying substitution at the bridging methylene position undergo a unique Electrochemical-Chemical (EC) process upon reduction from Rh(II) to Rh(I) as observed by cyclic voltammetry; transient electrogenerated Rh(I) species undergo a ligand rearrangement that results in facial η^2 coordination of one pyridine motif on the dpma platform. Studies of a family of [Cp*Rh] complexes bearing dimethyl- (Me_2dpma), dibenzyl- (Bn_2dpma), methyl,methylpyrenyl- (MePyrdpma), and bis(methylpyrenyl)- (Pyr_2dpma) substituted dpma ligands reveal a uniform trend in the first-order rate constants associated with this EC process involving ligand rearrangement, providing kinetic insight into a key process that enables stabilization of low-valent rhodium by substituted dpma-type ligands.

INTRODUCTION

Electrochemical studies offer a promising way of studying the chemistry of many transformations involving redox reactions or redox catalysis. The active forms of catalysts are often formed upon reduction by two or more electrons, generating transient intermediates near the electrode that have virtually zero bulk concentration.[1,2] As conventional spectroscopic studies of molecular electrocatalysis are difficult,[3] progress in many fields depends upon understanding electron transfer-induced reactivity with electrochemical methods.[4]

Indeed, as a cascading series of reactions are often possible for compounds that undergo multiple reductions, information on individual elementary reactions steps can be obscured by the multiple pathways often accessible at a given potential. A related further complication arises when follow-up chemical reactivity results in potential inversion of sequential reductions (as in ECE-type reactions).[5,6] Scheme 1 shows a series of reactions in a model catalytic cycle to illustrate these points. In this scheme, a model pre-catalyst, $[Cat_A]^{2+}$ is reduced by $1e^-$ to $[Cat_B]^+$, and $[Cat_B]^+$ then undergoes a subsequent $1e^-$ reduction to generate an electron-rich complex $[Cat_C]^0$. The low-valent $[Cat_C]^0$ species is of particular interest to us, since many redox reactions of contemporary relevance (H^+ reduction to H_2, CO_2 reduction to CO or other products) involve transfer of at least $2e^-$. Due to its nascent electron-rich nature, $[Cat_C]^0$ in our scheme undergoes a chemical reaction to generate a more stable form, $[Cat_D]^0$. Compounds like $[Cat_D]^0$ are notable, in that their formation after loading with multiple reducing equivalents is directly relevant to multielectron catalysis under reducing conditions.

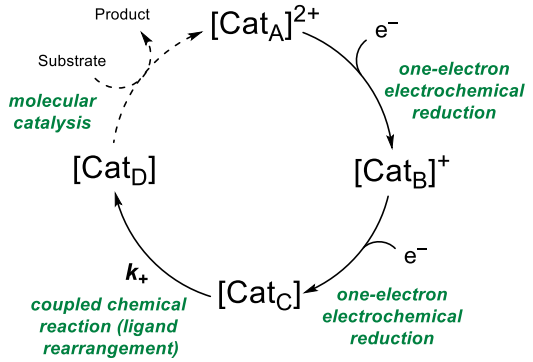

Scheme 1. General scheme for electrocatalysis

To serve as viable redox catalysts, metal complexes must bear ligands capable of supporting multiple metal/complex oxidation states. Non-innocent ligands that directly participate in redox chemistry are particularly noted for their ability to augment metal-based electron transfer and the resulting tendency to promote novel reactivity modes.[7] Ligands based upon the workhorse 2,2′-bipyridyl[8] (bpy) and pyridine-diimine[9] (PDI) cores are two such platforms, in which low-lying π^* molecular orbitals help stabilize reduced metal complexes.[10] PDI-based ligands can undergo multiple reduction events, obviating the need for metal-centered ET processes.[11] Similarly, the conjugated bpy ligand can accept electron density through π-backbonding[12,13] as well as directly accept electrons to generate reduced forms.[14] Such redox-active ligands and their compounds are common in molecular catalysis precisely because their properties help

stabilize the various charge states of intermediates. With stability supported across multiple oxidation states, catalytic intermediates become accessible and redox cycles can be constructed, even for complex multielectron reactions.

We have recently been exploring the synthetic chemistry of the dimethyl-2,2′-dipyridylmethane (Me_2dpma) ligand,[15] as we have found that Me_2dpma represents a notable counterpoint to the more common and well-studied bpy. In particular, disruption of the inter-ring conjugation found in bpy with Me_2dpma results in π^* orbitals that are less accessible for back-bonding or electron transfer as compared to those of bpy.[16] However, we have found that Me_2dpma is nonetheless capable of stabilizing reduced complexes. In particular, upon reduction of a model [Cp*Rh] complex (Cp* = η^5-pentamethylcyclopentadienyl) bearing κ^2-Me_2dpma to the formally Rh(I) oxidation state, one pyridyl ring of Me_2dpma rotates (flips) and facially coordinates to the Rh center in an η^2 fashion.[15] As demonstrated by crystallographic studies and complementary X-ray absorption spectroscopy, this rearrangement results in dearomatization of the flipped pyridyl ring and stabilization of the reduced metal center to a significant degree.[17]

$[Cp^*Rh(Me_2dpma)NCCH_3](PF_6)_2$ ($\mathbf{1}^{\mathbf{LMe2}}$) is amenable to electrochemical studies of this redox chemistry; avoidance of halide(s) precludes formation of $[Cp^*RhCl]_2$ following $1e^-$ reduction and enables accurate electrochemical studies.[15] Cyclic voltammograms (CVs) collected with this complex reflect the chemical reactivity described above. CVs reveal two discrete $1e^-$ reductions; the first $1e^-$ reduction is electrochemically quasi-reversible and chemically reversible, occurs at –0.85 V vs ferrocenium/ferrocene (denoted hereafter as $Fc^{+/0}$), and leads to generation of an isolable Rh(II) complex.[15] A second $1e^-$ reduction leads to generation of the formally Rh^I form of the compound ($E_{p,c}$ = –1.50 V vs. $Fc^{+/0}$). However, the appearance of the CVs confirm involvement of the reduction-induced chemical reaction in which Me_2dpma flips to stabilize the low-valent complex via η^2-coordination of one pyridine ring; the process appears electrochemically irreversible at lower scan rates but shows improved reversibility at faster scan rates. Thus, an Electrochemical-Chemical (EC) process is taking place, as defined by Nicholson and Shain[18] and studied extensively by Savéant.[19]

The well-defined chemistry and electrochemistry of $\mathbf{1}^{\mathbf{LMe2}}$ make it an attractive model for studying metal complexes that undergo EC processes. However, our prior work with this system bearing Me_2dpma was primarily chemical in nature. As our work has also been restricted solely to Me_2dpma (and its unsubstituted analogue dpma[20]), the role of the ligand substituents in influencing the noted reactivity and kinetics remain unclear. However, such information would clarify the electrochemical reaction sequence and provide new insight into a ligand-promoted charge stabilization process like those often needed in molecular catalysis. The coordination chemistry of dpma-type ligands has been limited to only a few examples on Cu,[21] Hg,[22] Pt,[23] Pd,[24] and Rh.[15,20] Notably, Schley and coworkers recently reported use of aryl-substituted dpma ligands in iridium catalysis, highlighting the usefulness and powerful tunability of these platforms.[25]

Here, we report the synthesis and characterization of a family of novel R_2dpma ligands ($\mathbf{LR_2}$, Chart 1) featuring substituents on the methylene "bridge" position and their [Cp*Rh^{III}] complexes ($\mathbf{1}^{\mathbf{LR2}}$, Scheme 2). We find the novel ligands $\mathbf{LBn_2}$, **LMePyr**, and $\mathbf{LPyr_2}$ are readily synthesized by methods designed to tolerate the benzylic C–H bonds present in the new derivatives.[27] Electrochemical studies indicate that, for all these complexes, reduction from Rh(II) to Rh(I) results in ligand reorientation and binding of one pyridine ring in an η^2 fashion. In line with this interpretation, reduction of $\mathbf{1}^{\mathbf{LBn2}}$ with Na(Hg) results in ligand rearrangement as shown via isolation and full characterization of the corresponding Rh(I) complex $\mathbf{4}^{\mathbf{LBn2}}$, confirming that the reactivity upon reduction tolerates bulkier, aromatic substituents on the dpma core and that the Rh–arene interactions are restricted to the pyridine motifs on the dpma ligand. However, digital simulations of the experimental cyclic voltammograms with DigiElch[26] reveal that the bulkier ligands undergo kinetically slower ligand reorientation, showing that ligand derivatization impacts the kinetics of reduction-induced dpma reorganization. Taken together, our findings show that disubstituted dpma ligands can stabilize multiple oxidation states and could thus be useful for developing new redox catalysts.

RESULTS AND DISCUSSION

Synthesis and Characterization of Ligands and [Cp*Rh] Complexes. The new substituted dipyridylmethane (dpma) ligands were synthesized based on modified literature procedures.[27,28] In prior work, treatment of dpma with sequential additions of nBuLi and MeI resulted in double methylation of the bridging methylene carbon of dpma. Here, we expanded upon this effective strategy by substituting other alkyl halides in place of methyl iodide in order to install sterically bulkier groups (see Chart 1) at the central methylene carbon. In order to prepare $\mathbf{LBn_2}$, the starting material bis(2-pyridyl)methane[29] was reacted with sequential additions of nBuLi and benzyl bromide. On the other hand, to prepare $\mathbf{LPyr_2}$, additions of tBuOK and 1-(chloromethyl)pyrene[30] were utilized; use of tBuOK in particular enabled preparation of $\mathbf{LPyr_2}$ whose immediate precursor features a pyrene ring that is more susceptible to undesired reactivity with the more nucleophilic nBuLi. The mixed derivative, **LMePyr**, was prepared analogously from 2,2′-(ethane-1,1-diyl)dipyridine[23] by treatment with single additions of tBuOK and 1-(chloromethyl)pyrene. This synthetic approach highlights that dpma ligands can be prepared via modular synthetic methods; in the case of our substituted dpma ligands, varying steric bulk can be installed above and below the plane containing the pyridyl rings.

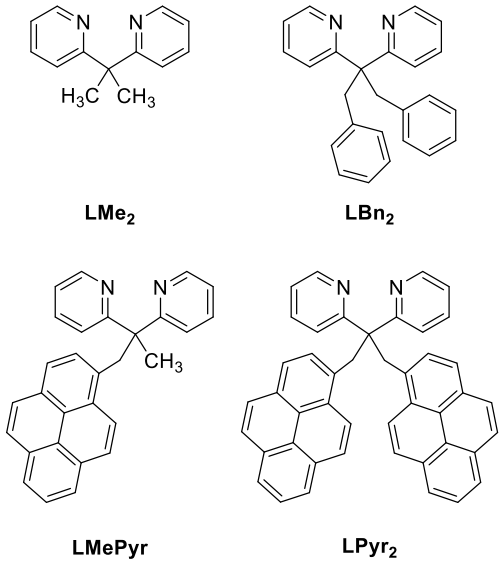

Chart 1. Substituted LR_2dpma ligands

The dimeric $[Cp^*RhCl_2]_2$ complex[31,32] is a generally useful precursor for the synthesis of $[Cp^*Rh]$ complexes bearing chelating bidentate ligands.[33] The family of $\mathbf{A}^{\mathbf{LR2}}$ complexes (Scheme 2) were prepared by addition of 1.0 equivalent of $AgPF_6$ to 0.5 equivalents of $[Cp^*RhCl_2]_2$ followed by the addition of 1.05 equivalents of the desired $\mathbf{LR_2}$ ligand to yield rhodium(III) complexes as orange solids. The $\mathbf{A}^{\mathbf{LR2}}$ compounds were very stable in our hands, and thus our initial characterization efforts focused on these derivatives. However, treatment of the $\mathbf{A}^{\mathbf{LR2}}$ complexes with 1.0 equivalent of $AgPF_6$ in CH_3CN results in rapid formation of the corresponding yellow solvento complexes $\mathbf{1}^{\mathbf{LR2}}$; while isolation of these species is challenging due to the lability of the bound solvent molecule, these solvento complexes lack a halide ligand, and were therefore utilized in the electrochemical studies to avoid electrochemically-induced generation of $[Cp^*RhCl]_2$ (*vide infra*).

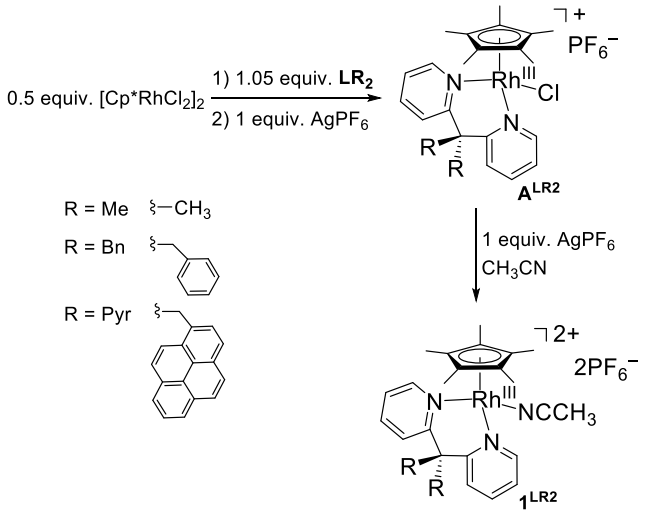

Scheme 2. Synthesis of series of $\mathbf{1}^{\mathbf{LR2}}$ Rh complexes.

Following isolation of the $\mathbf{A}^{\mathbf{LR2}}$ complexes, proton nuclear magnetic resonance (^{1}H NMR) was used to confirm chelation of the new disubstituted dpma ligands to rhodium. In the cases of all the new complexes, a strong singlet appears at ca. 1.60 ppm; this resonance is attributable to the fifteen equivalent protons associated with the freely rotating $[Cp^*]$ ligand and integrates to 15H with respect to the two *ortho*-pyridyl protons of the associated κ^2-$\mathbf{LR_2}$ ligand (Figures S7, S12, S19). Additionally, the $^{31}P\{^1H\}$ NMR spectra of the complexes **A** reveal a septet attributable to the presence of the hexafluorophosphate counteranion ($^1J_{P,F} \approx 706$ Hz). The ^{1}H NMR spectrum for $\mathbf{A}^{\mathbf{LBn2}}$ reveals two unique singlets integrating to 2H each (3.85 and 3.67 ppm) corresponding to the chemically inequivalent methylene protons associated with each of the freely rotating benzyl substituents. These signals contrast with the single ^{1}H NMR resonance at 4.52 ppm (integrating to 4H) associated with the four equivalent methylene protons of the free $\mathbf{LBn_2}$ ligand.

On the other hand, the ^{1}H NMR spectrum of $\mathbf{A}^{\mathbf{LPyr2}}$ reveals a more complex case in which three unique resonances associated with the methylene protons of the methylpyrenyl substituents are observed. One singlet at 4.66 ppm integrates to 2H, corresponding to one set of methylene protons associated with the methylpyrenyl substituent pointing away from $[Cp^*]$ which can freely rotate. Two further doublets are present at 6.28 and 6.59 ppm integrating to 1H each, corresponding to the two methylene protons on the methylpyrenyl substituent which points toward $[Cp^*]$. These protons are chemically inequivalent, presumably due to hindered rotation of the upper methylpyrenyl substituent which would encounter steric clash if fully rotated upward, as can be estimated based on the solid-state structure of $\mathbf{A}^{\mathbf{LPyr2}}$ (vide infra). These methylene protons exhibit the expected geminal coupling to each other ($^2J_{H,H} \approx 8.1$ Hz) resulting in the measured doublet resonances.

The ^{1}H NMR spectrum for the non-symmetrically substituted free **LMePyr** ligand reveals a singlet integrating to 2H at 4.56 ppm that corresponds to the two equivalent methylene protons of the single methylpyrenyl substituent; another singlet at 1.63 ppm integrates to 3H and corresponds to the methyl substituent. In the spectrum of $\mathbf{A}^{\mathbf{LMePyr}}$, this singlet corresponding to the methyl substituent shifts to 1.73 ppm. The methylene protons for the methylpyrenyl substituent, however, are detected in this case as two broad singlets at 5.02 and 4.14 ppm; this is again indicative of hindered rotation of the methylpyrenyl substituent when **LMePyr** is bound to $[Cp^*Rh]$. This stereochemical assignment, which predicts that the methylpyrenyl substituent is facing toward the $[Cp^*]$ ligand, is confirmed by the X-ray diffraction studies described below; it is also supported by detectable through-space coupling that occurs between the protons of the pyrenyl group and $[Cp^*]$ methyl groups in NOESY NMR of $\mathbf{A}^{\mathbf{LMePyr}}$ (see SI, Figure S17). Taken together, the NMR data thus confirm the presence of the bidentate dpma ligands on the $[Cp^*Rh]$ for the new complexes.

Vapor diffusion of diethyl ether (Et_2O) into an acetonitrile (CH_3CN) solution containing $\mathbf{A}^{\mathbf{LBn2}}$ or CH_2Cl_2 solutions of $\mathbf{A}^{\mathbf{LMePyr}}$ and $\mathbf{A}^{\mathbf{LPyr2}}$ afforded orange crystals suitable for X-ray diffraction (XRD) studies. The resulting solid-state structures (see Figure 1) reveal the geometries of the formally Rh(III) metal centers in all three complexes to be *pseudo*-octahedral. The first coordination sphere around each Rh center contains the appropriate κ^2-[*N,N*]-disubstituted dpma ligand, a single chloride anion, and the $[\eta^5$-$Cp^*]$ ligand. The bond metrics (Table 1) for the new structures reported here compare well with those for the previously investigated derivative $\mathbf{A}^{\mathbf{Me2}}$, suggesting that the more sterically demanding ligands developed here do not markedly perturb the properties of the Rh(III) center. The N1-Rh-N2 chelate angles (Table 2) do not vary significantly, either, suggesting there only a subtle influence from the presence of the two more sterically demanding aromatic substituents in

these cases. And, as mentioned above, the structure of $\mathbf{A}^{\mathbf{LMePyr}}$ confirms that the methylpyrenyl substituent is oriented toward [Cp*] as predicted on the basis of NMR data (*vide supra*).

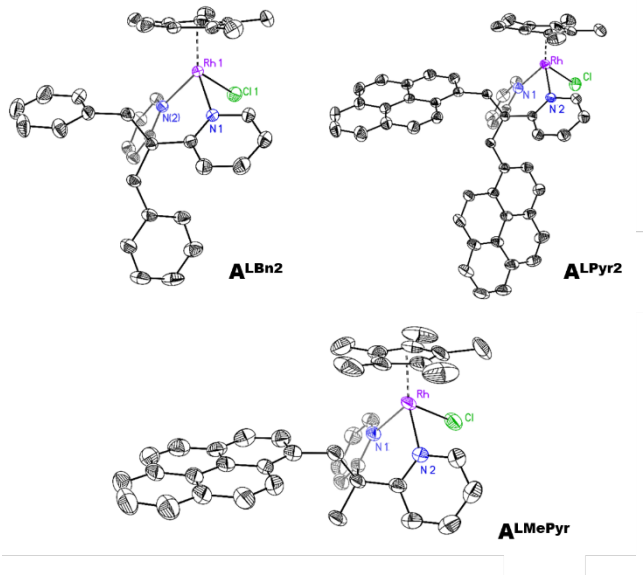

Figure 1. Solid-state structure of $\mathbf{A}^{\mathbf{LBn2}}$, $\mathbf{A}^{\mathbf{LPyr2}}$, and $\mathbf{A}^{\mathbf{LMePyr}}$ (XRD). Hexafluorophosphate counteranion and hydrogen atoms are omitted for clarity. Thermal ellipsoids are shown at the 50% probability level.

The angle between the chelation plane of the bidentate ligand (a plane defined by the positions of the N1, N2, and Rh atoms) and the plane defined by the [η^5-Cp*] ligand is similar across the series (66.27–66.77°), except for the case of $\mathbf{A}^{\mathbf{LPyr2}}$ which displays a narrower angle of 64.78°. The uniqueness of $\mathbf{A}^{\mathbf{LPyr2}}$ is attributable to the steric bulk of the second methylpyrenyl substituent, which causes a marginally significant distortion of the first coordination sphere about Rh. Accordingly, all these angles are significantly greater than the analogous value for $[Cp^*Rh(bpy)Cl]^+$ (~59°)[34]; this is consistent with the greater out-of-plane steric bulk of all the κ^2-R_2dpma ligands here in comparison with κ^2-bpy ligand.

	Rh-N (Å)	Rh-Cp*(Å)	∠N1-Rh-N2	∠Cp*-dpma	Ref.
$\mathbf{A}^{\mathbf{LMe2}}$	2.130(2), 2.133(2)	1.803	85.44(8)°	66.77°	Ref. 15
$\mathbf{A}^{\mathbf{LBn2}}$	2.112(2), 2.122(2)	1.811	84.03(8)°	66.37°	This work
$\mathbf{A}^{\mathbf{LMePyr}}$	2.125(3), 2.135(3)	1.809	85.30(2)°	66.27°	This work
$\mathbf{A}^{\mathbf{LPyr2}}$	2.118(3), 2.120(3)	1.810	85.10(2)°	64.78°	This work

Table 1. Tabulated bond lengths and angles of $\mathbf{A}^{\mathbf{LR2}}$ found from XRD.

Our previous studies have shown that $[Cp^*Rh(Me_2dpma)NCCH_3](PF_6)_2$ ($\mathbf{1}^{\mathbf{LMe2}}$) has a unique electrochemical profile in which a distinct Electrochemical-Chemical (EC) process is observable upon reduction of the system from Rh(II) to Rh(I).[13,15] A similar profile was observed here for the new series of $\mathbf{1}^{\mathbf{LR2}}$ complexes (Figure 2.) The $\mathbf{1}^{\mathbf{LR2}}$ complexes, which are the acetonitrile solvento analogues of the chloride-bound $\mathbf{A}^{\mathbf{LR2}}$ precursors described above, were used in the electrochemical studies to avoid a detrimental side reaction observed in the presence of chloride.[15] The $\mathbf{1}^{\mathbf{LR2}}$ complexes could be cleanly generated in all cases with the addition of one equivalent of $AgPF_6$ (Scheme 2) to the corresponding $\mathbf{A}^{\mathbf{LR2}}$ complexes. The $\mathbf{A}^{\mathbf{LR2}}$ complexes were fully characterized by ^{1}H, ^{13}C{^{1}H}, ^{31}P{^{1}H} and ^{19}F NMR, elemental analysis and XRD, while the more sensitive $\mathbf{1}^{\mathbf{LR2}}$ complexes, on the other hand, were characterized solely by ^{1}H NMR to confirm full conversion of $\mathbf{A}^{\mathbf{LR2}}$ to $\mathbf{1}^{\mathbf{LR2}}$ after *in situ* generation and isolation for immediate use in the electrochemical studies. The complexes $\mathbf{1}^{\mathbf{LR2}}$ were studied as opposed to complexes $\mathbf{A}^{\mathbf{LR2}}$ to avoid the formation $[Cp^*RhCl]_2$ complex following 1e$^-$ reduction observed in electrochemical studies conducted in the presence of chloride/halide ligands that promote dimerization.

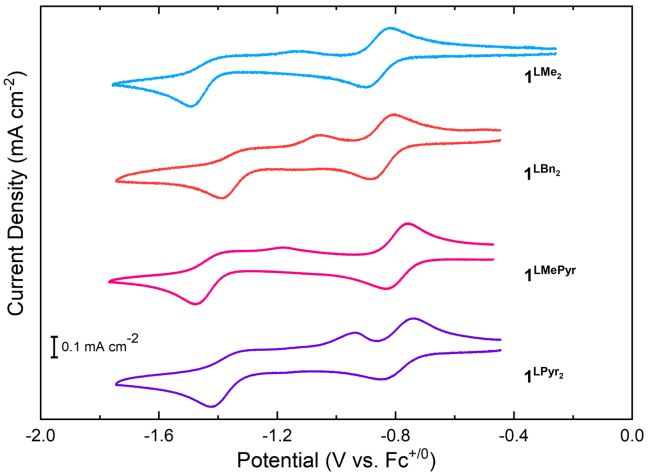

Figure 2. Cyclic voltammetry of $\mathbf{1}^{\mathbf{LMe2}}$ (blue), $\mathbf{1}^{\mathbf{LBn2}}$ (red), and $\mathbf{1}^{\mathbf{LMePyr}}$ (pink) and $\mathbf{1}^{\mathbf{LPyr2}}$ (purple). Conditions: Electrolyte, 0.1 M $TBAPF_6$ in CH_3CN; scan rate, 50 mV/s; working electrode, highly oriented pyrolytic graphite (HOPG); [Rh] in each experiment ca. 1 mM. Initial potentials $\mathbf{1}^{\mathbf{LMe2}}$, ca. – 0.5 V; $1^{\mathbf{LR2}}$, ca. – 0.4 V.

Cyclic voltammetric studies of solutions containing the $\mathbf{1}^{\mathbf{LR2}}$ complexes reveal similar cathodic and anodic events in each case (Figure 2), in line with our initial chemical and electrochemical studies of $\mathbf{1}^{\mathbf{LMe2}}$. With a high degree of similarity to that of $\mathbf{1}^{\mathbf{LMe2}}$, the cyclic voltammogram of $\mathbf{1}^{\mathbf{LBn2}}$ reveals that initial quasi-reversible 1e$^-$ reduction ($E_{1/2}$ (Rh^{III}/Rh^{II}) = –0.84 V) that leads to generation of $\mathbf{2}^{\mathbf{LBn2}}$ (Scheme 3). A second 1e$^-$ reduction is observed at a more negative potential ($E_{pc}(Rh^{II}/Rh^{I})$= –1.40 V); this process appears fully irreversible at lower scan rates, implicating the relatively rapid conversion of the nascent $\mathbf{3}^{\mathbf{LBn2}}$ (a formally Rh(I) form bearing κ^2-Bn_2dpma) into $\mathbf{4}^{\mathbf{LBn2}}$ (bearing the flipped version of the ligand with an η^2 pyridine ring; see Scheme 3 for structures of all these compounds).[15] Consistent with stabilization of the reduced Rh center by the rearrangement of the pyridine ring, the return anodic scan reveals a coupled irreversible oxidation ($E_{p,a}(Rh^{I}\rightarrow Rh^{II})$ = –1.05 V) that leads to regeneration of $\mathbf{2}^{\mathbf{LBn2}}$ via oxidation of $\mathbf{4}^{\mathbf{LBn2}}$ followed by reorientation of the Bn_2dpma ligand to the original κ^2 configuration. This model for the cyclic voltammetric response of $\mathbf{1}^{\mathbf{LBn2}}$ is consistent with the high degree of reversibility of the initial Rh^{III}/Rh^{II} couple, since $\mathbf{2}^{\mathbf{LBn2}}$ is cleanly regenerated by the proposed anodic reaction sequence. The model is also supported by the anodic electrochemical behavior of isolated $\mathbf{4}^{\mathbf{LBn2}}$ (*vide infra*), which shows two oxidation events (see SI, Figures S35 and S36) that closely mirror those displayed in cyclic voltammetry experiments carried out with $\mathbf{1}^{\mathbf{LBn2}}$. The voltammetric responses of $\mathbf{1}^{\mathbf{LMePyr}}$ and $\mathbf{1}^{\mathbf{LPyr2}}$ closely mirror those of $\mathbf{1}^{\mathbf{LMe2}}$ and $\mathbf{1}^{\mathbf{LBn2}}$; a minor broadening of the cathodic and anodic waves for $\mathbf{1}^{\mathbf{LPyr2}}$, as well as a slight apparent increase in the diffusion

coefficient for the pyrene-appended compounds (see SI, Table S2), may implicate interactions between the carbon working electrode surface and the compound engendered by the extended aromatic π system of the pyrene groups. $\mathbf{1}^{\mathbf{LBn2}}$, $\mathbf{1}^{\mathbf{LMePyr}}$, and$\mathbf{1}^{\mathbf{LPyr2}}$ were all found to be freely diffusing on the basis of scan rate dependence cyclic voltammetry studies (see SI, Figures S30, S33, S38, S41).

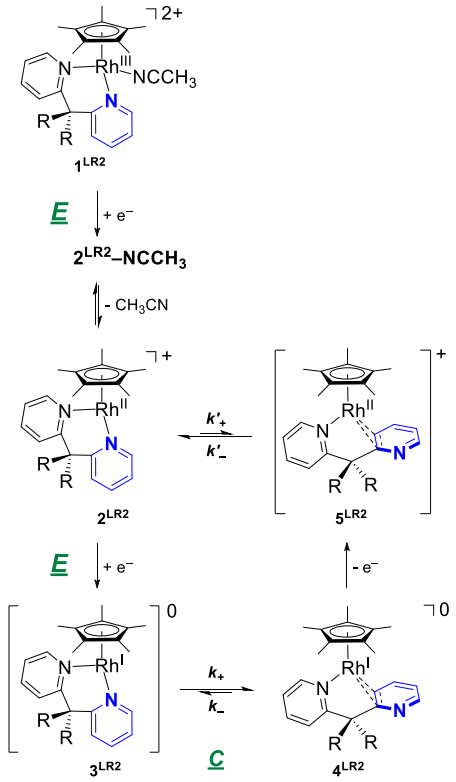

Scheme 3. Electrochemical reduction scheme for the family of $\mathbf{1}^{\mathbf{LR2}}$ complexes.

The values of the midpoint potential for the initial quasi-reversible Rh^{III}/Rh^{II} reduction among the series of $\mathbf{1}^{\mathbf{LR2}}$ complexes show that there is a slight electronic dependence based on the electron-donating or -withdrawing properties of the substituents appended to the LR_2 backbone (Table 2). $\mathbf{1}^{\mathbf{LMe2}}$, which features the most electron-donating substituents, two methyl groups, has the most negative Rh^{III}/Rh^{II} potential ($E_{1/2}$ = –0.86 V vs. $Fc^{+/0}$). $\mathbf{1}^{\mathbf{LBn2}}$ has the next more-positive reduction potential ($E_{1/2}$ = –0.84 V vs. $Fc^{+/0}$), consistent with the presence of the more electron-withdrawing aromatic benzyl substituents.[35] The most positive reduction potentials in the series are associated with the methylpyrenyl substituted $\mathbf{1}^{\mathbf{LMePyr}}$ and $\mathbf{1}^{\mathbf{LPyr2}}$ complexes ($E_{1/2}$ = – 0.80 V vs. $Fc^{+/0}$). This is consistent with the presence of the large aromatic π-system in the pyrenyl functionalities, which can be expected to be the most electron-withdrawing. Notably, there is no significant trend among the E_{pa} and E_{pc} values associated with the Rh^{II}/Rh^{I} redox events in the series of complexes, suggesting that the electronic influence of the ligand substituents does not strongly affect the peak potentials associated with Rh^{II}/Rh^{I} interconversion.

	$E_{1/2}$ $Rh^{III/II}$	ΔE_p $Rh^{III/II}$	E_{pc} $Rh^{II/I}$	E_{pa} $Rh^{II/I}$
$\mathbf{1}^{\mathbf{LMe2}}$	–0.86 V	78 mV	–1.45 V	–1.02 V
$\mathbf{1}^{\mathbf{LBn2}}$	–0.84 V	79 mV	–1.40 V	–1.05 V
$\mathbf{1}^{\mathbf{LMePyr}}$	–0.80 V	72 mV	–1.48 V	–1.17 V
$\mathbf{1}^{\mathbf{LPyr2}}$	–0.80 V	109 mV	–1.43 V	–0.93 V

Table 2. Reduction potentials for series of $\mathbf{1}^{\mathbf{LR2}}$ complexes.

Further support for the reaction sequence outlined in Scheme 3 is provided by the chemical isolation (see Experimental Section) and structure of $\mathbf{4}^{\mathbf{LBn2}}$ obtained from XRD analysis (Figure 3). These data confirm that the structural rearrangement of the ligand that results in η^2 pyridine coordination upon reduction of the compound to the Rh^{I} oxidation state remains operative even when aryl substituents are appended to the ligand backbone that could alternatively interact with the metal center in the reduced form of the complex. Indeed, we find that one of the pyridine moieties of $\mathbf{4}^{\mathbf{LBn2}}$ binds to the Rh center in a closely similar fashion as in the $\mathbf{4}^{\mathbf{LMe2}}$ complex[15] in which the Rh center interacts with pyridine and effectively dearomatizes the ring. Analogous to the bonding metrics in $\mathbf{4}^{\mathbf{LMe2}}$, the Rh center is within bonding distance of C10 (C10–Rh: 2.065(2) Å) and C9 (C9–Rh 2.113(2) Å) attesting to the ligation of Rh to the C9–C10 olefin. Indicative of the bonding within the pyridine ring of $\mathbf{4}^{\mathbf{LBn2}}$, the C9–C10 bond elongates in comparison to the length found in $\mathbf{1}^{\mathbf{LBn2}}$ as a result of strong π-backbonding. Dearomatization of the heterocycle results in localization of double bond character within the ring, comparable to the case of $\mathbf{4}^{\mathbf{LMe2}}$ in which alternating short/long C–C/C–N bond distances are observed (Figure 3). A remarkable feature observed in the $\mathbf{4}^{\mathbf{LBn2}}$ XRD structure is the significant pyramidalization of C10, consistent with the upfield shift in the ^{1}H NMR of H10 (SI Figure S24) consistent with the anticipated sp^3-hybridization of C10 in both structures.[15] Notably, NMR studies corroborate the XRD finding that one of the pyridine motifs on the dpma framework is the only arene ligand interacting with Rh even in the presence of other aromatic fragments. Based on the bonding metrics measured for $\mathbf{4}^{\mathbf{LBn2}}$ and $\mathbf{4}^{\mathbf{LMe2}}$, we reason that the Rh center in $\mathbf{4}^{\mathbf{LBn2}}$ interacts with its olefinic ligand in a similar to manner to that in $\mathbf{4}^{\mathbf{LMe2}}$. Thus, metal-to-olefin backdonation within the context of the Dewar-Chatt-Duncanson[17] model stabilizes the formally Rh^{I} center in both cases.[15] Multiple attempts to isolate the $2e^-$ reduced forms of the $\mathbf{A}^{\mathbf{LMePyr}}$ and $\mathbf{A}^{\mathbf{LPyr2}}$ complexes were unsuccessful, due to cogeneration of side products with similar solubility profiles following chemical reduction.

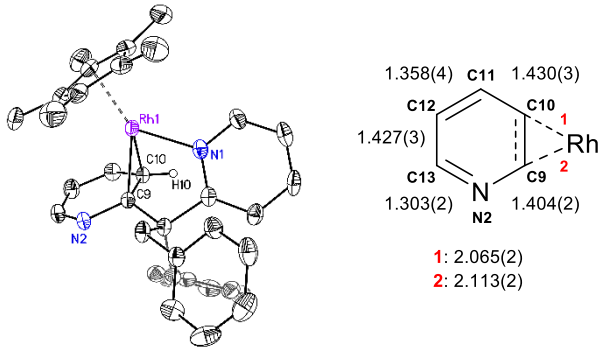

Figure 3. Solid-state structure of $\mathbf{4}^{\mathbf{LBn2}}$ (XRD) and selected bond metrics (Å). Hydrogen atoms (except H10) are omitted for clarity. Thermal ellipsoids are shown at the 50% probability level.

Upon observing the analogous EC processes for the various $\mathbf{1}^{\mathbf{LR2}}$ complexes resembling the process encountered in our prior studies with the $\mathbf{LMe_2}$-ligated complex, we next endeavored to quantify the rate of the redox-induced ligand rearrangement observed for conversion of $\mathbf{3}^{\mathbf{LR2}}$ to $\mathbf{4}^{\mathbf{LR2}}$ (Scheme 3). In cases where a redox process involves an EC mechanism, the current corresponding to re-oxidation of the reduced form of a given compound is negligible at slower scan rates, since the immediate product of reduction is consumed by the coupled chemical reaction before it can undergo reoxidation on the return anodic sweep. In order to understand this situation and analyze the rate of ligand rearrangement, we turned to the Zone Diagrams for electrochemical analysis developed by Savéant.[19] Savéant has used Zone Diagrams for general cases of the EC mechanism to understand the competition between the rate of diffusion, the properties of the redox induced chemical reaction (as a function of its equilibrium constant K) and a dimensionless parameter, λ, which describes the competition between the rate of the coupled chemical reaction and the rate of diffusion. The dimensionless parameter λ is inversely dependent upon the scan rate at which the cyclic voltammogram is measured. Therefore, as illustrated in the Zone Diagrams,[19] as the scan rate of the voltammetry is increased, the dimensionless parameter λ decreases. As λ decreases, the reduced form of the metal complex is allowed less time to diffuse in solution, and as a result, less time is allotted for the chemical process involved to occur. Thus, at the higher scan rates, the peak current associated with re-oxidation of the reduced form of the complex on the anodic sweep increases until it reaches a maximum value under conditions where the coupled chemical reaction has insufficient time to affect the appearance of the voltammetric data.

In order to provide the experimental data needed to quantify the rate of the ligand rearrangement of interest here, we performed cyclic voltammetry with each complex $\mathbf{1}^{\mathbf{LR2}}$ over a wide range of scan rates. Taking $\mathbf{1}^{\mathbf{LBn2}}$ as an example, Figure 4 shows selected voltammograms of the compound taken at 50, 1000, and 2500 mV/s. The second reduction in the data exhibits the tell-tale characteristics of an EC mechanism; the expected increase in the cathodic peak current with increasing scan rate (increasing with a square root dependence per the Randles-Ševćik equation[36]) at E_{pc} = –1.40 V vs $Fc^{+/0}$ is associated with observation of a corresponding anodic process only at higher scan rates. At a slower scan rate, the dimensionless parameter λ is large, meaning that the system has ample time for the reduction-induced chemical reaction to occur. Conversely, at higher scan rates we observe the appearance of the re-oxidation coupled to the most negative reduction event, corresponding to the presence of a now electrochemically quasi-reversible process. This increase in anodic current is a direct result of the influence of the dimensionless parameter λ now having a smaller value, meaning at the faster scan rate we can overcome the rate of the diffusion and the rate of the chemical reaction to re-oxidize the reduced form of the compound. By this method we can measure the rate of the reduction-induced reaction observed by CV. Analogous scan rate dependent studies yielded similar behavior for each of the complexes $\mathbf{1}^{\mathbf{LR2}}$ in the series (Figures S31, S34, S39, S42).

The rate constant for the chemical step in the EC process described above was taken as the target of our analysis. In order to measure this first-order rate constant (k_+) for the ligand reorientation/flip chemical step (see Scheme 3), we turned to digital simulation of our CVs since the well-resolved nature of the redox processes enable us to clearly model the data (Figure 5).[26] To examine the rate constant of the EC process, we focused on the anodic return wave that is a result of the oxidation of the doubly reduced complex outpacing the coupled chemical reaction. This anodic feature directly reports on the value of λ. In order to extract the value of k_+, we simulated our entire library of scan rate dependent cyclic voltammograms at which the anodic return wave was measurable, in order to capture the increasing chemical reversibility of the redox process involving our chemical reaction of interest (see Scheme 3). Notably, within our model, the value of k_+ is independent of scan rate and concentration (at all scan rates, see SI Figures S54 and S55) even though the value of λ does change at each scan rate, giving rise to the variable appearance of the data. The chemical properties of the system were thus interrogated at all of the scan rates for which a return wave is observable ($\mathbf{1}^{\mathbf{LR2}}$: 300–2500 mV/s, $\mathbf{1}^{\mathbf{LPyr2}}$: 250–2000 mV/s, see SI Figure S44, S47-S53).

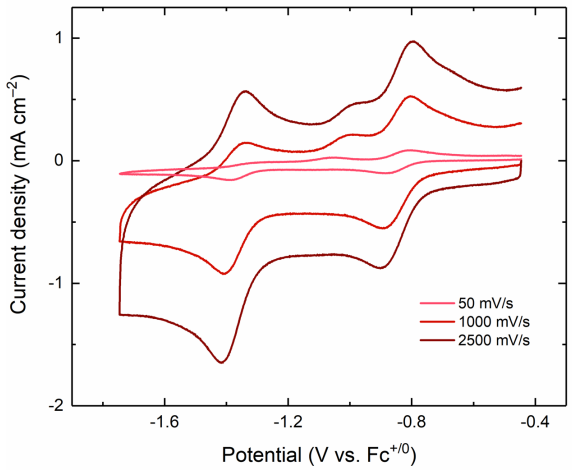

Figure 4. Cyclic voltammetry of $\mathbf{1}^{\mathbf{LBn2}}$ at increasing scan rates. Conditions: Electrolyte, 0.1 M $TBAPF_6$ in CH_3CN; working electrode, highly oriented pyrolytic graphite (HOPG); [Rh] in each experiment ca. 1 mM.

To extract the kinetic information from the simulated data for our compounds, the reaction sequence given in Scheme 3 was programmed into DigiElch. Additionally, experimentally determined values for certain variables were added to the model as needed, including the following: the double layer capacitance of the highly oriented pyrolytic graphite (HOPG) working electrode (determined via scan rate dependence of electrode background currents in our 0.1 M $TBAPF_6/CH_3CN$ electrolyte; 1.0 x 10^{-5} F) (see SI, Figure S43); the solution resistance determined at several applied voltages (c.a. 110 –150 Ω); the area of the HOPG working electrode (0.09 mm^2); the temperature (298 K); and the concentration of the given $\mathbf{1}^{\mathbf{LR2}}$ compound in solution (ca. 10^{-3} M). Based on the appearance of the voltammetry, the initial value of the charge transfer coefficient, α, was set to 0.5 in all cases. The potentials shown in Table 2 ($E_{1/2}$, E_{pa}, E_{pc}), obtained from inspection of the initial voltammetric data were also input as starting points for the simulation software to fit the reduction potentials internally. Following optimization, the reduction potentials determined by DigiElch matched well with those determined manually by inspection of the data (see SI, Figures S44, S47-S53). With this approach, we were able to determine the k_+ values for the target EC process (see Scheme 3 and Table 3). Reasonable values were also extracted for diffusion coefficients (cm^2/s) and heterogenous electron transfer rates (k°, cm/s) for each of the $\mathbf{1}^{\mathbf{LR2}}$ complexes (see SI, Table S2).

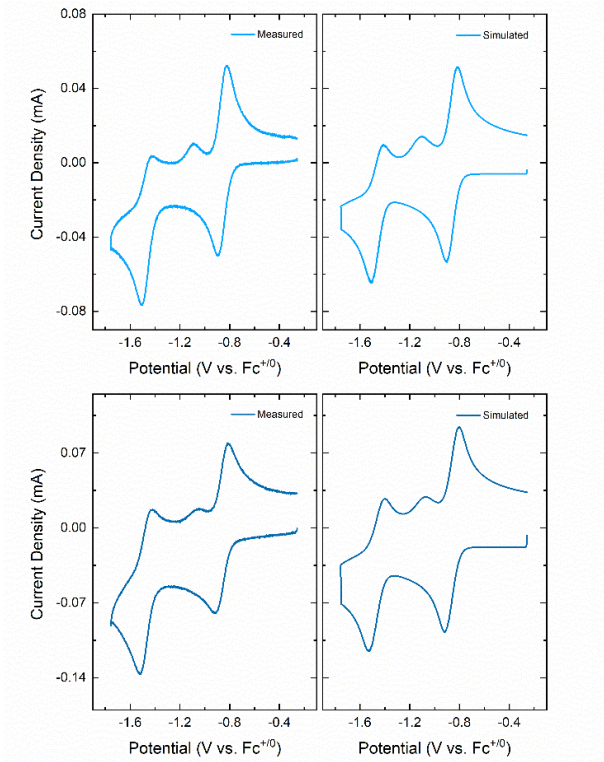

Figure 5. Measured (left) and simulated (right) CV of $\mathbf{1}^{\mathbf{LMe2}}$. Scan rates of 500 mV/s (upper), and 1500 mV/s (lower). Measured CV conditions: Electrolyte, 0.1 M TBAPF6 in CH_3CN; working electrode, highly oriented pyrolytic graphite (HOPG); [Rh] in each experiment ca. 1 mM. Initial potentials ca. −0.5 V. Simulated CV conditions: mechanism in shown in Scheme 3; reduction potentials (Table 2); double layer capacitance 1.0 x 10^{-5} F (Figure S43); resistance c.a. 110 −150 Ω; working electrode area 0.09 cm^2; temperature 298 K; concentration c.a.1 mM.

Based on the results of the simulations, a distinct relationship between k_+ and the steric bulk of the substituents on the methylene bridge (Table 3) can be observed. We find that the least sterically bulky methyl substituents in $\mathbf{1}^{\mathbf{LMe2}}$ engender the fastest ligand rearrangement with $k_+ = 1.65 \pm 0.08$ s^{-1}. The $\mathbf{1}^{\mathbf{LBn2}}$ complex, featuring the more sterically bulky benzyl substituents, has $k_+ = 1.31 \pm 0.19$ s^{-1} which is slower. $\mathbf{1}^{\mathbf{LMePyr}}$ complex, featuring single methylpyrenyl and methyl moieties, displays a significantly slower rate of the ligand flip with $k_+ = 0.60 \pm 0.14$ s^{-1}. The pyrene moiety features a considerably larger steric profile than the other substituents in this family of complexes, and as a result, the k_+ value associated with the EC process for $\mathbf{1}^{\mathbf{LMePyr}}$ is significantly slowed compared to the other derivatives. The value of k_+ for $\mathbf{1}^{\mathbf{LPyr2}}$ is even smaller at 0.16 ± 0.01 s^{-1}, supporting the notion that the steric bulk of the substituents appended to the methylene bridge of the **LR2** ligands influences the rate of the ligand flip giving rise to stabilization of the Rh^I oxidation state. The k_+ measured for the $\mathbf{1}^{\mathbf{LPyr2}}$ EC process is an entire order of magnitude slower than that observed for $\mathbf{1}^{\mathbf{LMe2}}$. Taken together, the simulations indicate that the substituents' steric bulk affects how long it takes to interconvert between intermediates upon reduction; greater steric bulk inhibits the rate of the ligand flip of the single pyridine moiety. Appealingly, the results show that the rates determined by digital simulation are significantly different from one another (see SI Figure S55). Confirming the first-order nature of the ligand reorientation/flip step, the value of k_+ was found to be independent of the solution concentration of $\mathbf{1}^{\mathbf{LR2}}$ (see SI, Figure S54).

	$\mathbf{1}^{\mathbf{LMe2}}$	$\mathbf{1}^{\mathbf{LBn2}}$	$\mathbf{1}^{\mathbf{LMePyr}}$	$\mathbf{1}^{\mathbf{LPyr2}}$
k_+ (s^{-1})	1.65 ± 0.08	1.31 ± 0.19	0.60 ± 0.14	0.16 ± 0.01

Table 3. First order rate constants (k_+) for the EC process observed for the family of complexes. Error bars are shown as ±1 σ and were determined by replicate measurements/simulations at the various scan rates given in the main text.

These findings are of potential relevance to the development of new ligand frameworks for use in molecular electrocatalysis, as (pre)catalysts prepared with sterically bulky substituents may be prone to slow interconversion between intermediates. Use of bulky ligand substituents is especially likely in cases where a given catalyst is incorporated into elaborate supramolecular constructs; electrode surface attachment schemes and use of chromophore-catalyst assemblies are two examples of such situations. In these cases, the interconversion of intermediates could impact the expected catalysis, since simpler model compounds may not reflect the kinetic properties of highly functionalized analogues.[37,38] Along a similar line, the attachment of functionalities in the second coordination sphere (like acids or bases) via tethering groups could slow reactions following redox activation steps.[39] In particular, the kinetics of formation of the species $\mathbf{4}^{\mathbf{LR2}}$ here that feature η^2-pyridyl ligands are of particular interest to us, since low-valent organometallic complexes are especially promiscuous in adopting a variety of coordination modes with carbon-based ligands.[40] Monitoring changes in coordination mode(s) and activation of substrates by electrochemical means offers interesting opportunities to develop new reaction schemes amenable to use in molecular electrocatalysis.

CONCLUSIONS

We find that transient Rh^I species bearing substituted κ^2-dpma ligands undergo a unique Electrochemical-Chemical (EC) process in cyclic voltammetry upon reduction from Rh(II) to Rh(I); transient electrogenerated Rh(I) species undergo a ligand rearrangement that results in facial η^2 coordination of one pyridine motif. Our studies indicate that the introduction of sterically bulky substituents engenders significant changes in the first-order rate constant associated with the chemical step of the noted EC process (k_+). We find that the steric bulk engendered by the $\mathbf{1}^{\mathbf{LPyr2}}$ systems slows k_+ by an order of magnitude compared to the value measured with $\mathbf{1}^{\mathbf{LMe2}}$. This study represents a relatively uncommon case where a series of elementary rate constants could be well quantified via modeling of scan rate-dependent electrochemistry data collected under readily accessible conditions (Scheme 4). Thus, we anticipate that our findings could be of use in interpretation of results from other systems where more complex reactivity may preclude direct measurement of individual elementary rate constants, such as in systems where molecular electrocatalysis is taking place.

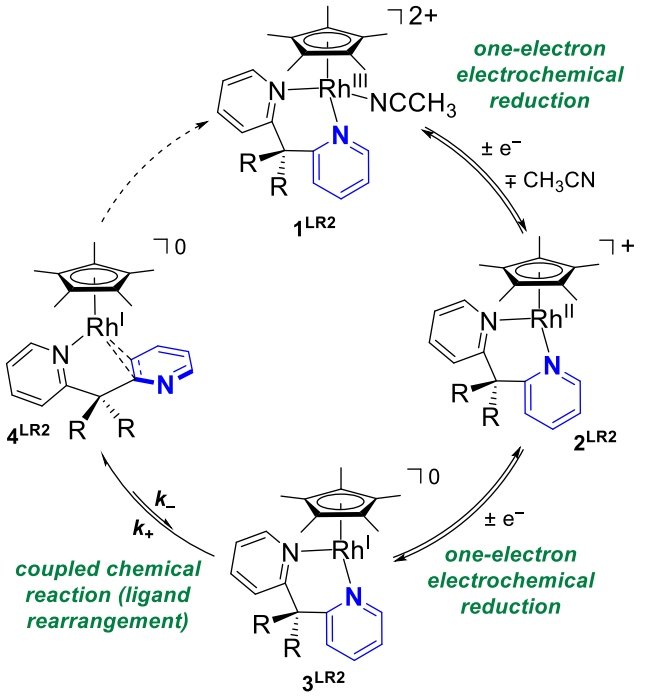

Scheme 4. Reactivity pathway measured for the family of [Cp*Rh] complexes.

EXPERIMENTAL SECTION

General Considerations. All manipulations were carried out in dry N_2-filled gloveboxes (Vacuum Atmospheres Co., Hawthorne, CA) or under N_2 atmosphere using standard Schlenk techniques unless otherwise noted. All solvents were of commercial grade and dried over activated alumina using a PPT Glass Contour (Nashua, NH) solvent purification system prior to use, and were stored over molecular sieves. All chemicals were from major commercial suppliers and used as received after extensive drying. $[Cp^*RhCl_2]_2$ was prepared according to literature procedures.[31,32] The substituted dpma ligands were synthesized by the methods of Canty and Mohr.[27] Bis(2-pyridyl)methane, 2,2′-(ethane-1,1-diyl)dipyridine, and 1-(chloromethyl)pyrene were also prepared according to literature methods.[23,29,30]

Deuterated NMR solvents were purchased from Cambridge Isotope Laboratories; CD_3CN was dried over molecular sieves and C_6D_6 was dried over sodium/benzophenone. ^1H, ^{13}C, and ^{19}F NMR spectra were collected on 400 or 500 MHz Bruker spectrometers and referenced to the residual protio-solvent signal[41] in the case of ^1H and ^{13}C. Heteronuclear NMR spectra were referenced to the appropriate external standard following the recommended scale based on ratios of absolute frequencies (Ξ).[42] ^{19}F NMR spectra are reported relative to CCl_3F. Chemical shifts (δ) are reported in units of ppm and coupling constants (J) are reported in Hz. Electronic absorption spectra were collected with an Ocean Optics Flame spectrometer and 1-cm pathlength quartz cuvettes. Elemental analyses were performed by Midwest Microlab, Inc. (Indianapolis, IN).

Electrochemistry. Electrochemical experiments were carried out in a nitrogen-filled glove box. 0.10 M tetra(n-butylammonium)hexafluorophosphate (Sigma-Aldrich; electrochemical grade) in acetonitrile served as the supporting electrolyte. Measurements were made with a Gamry Reference 600 Plus Potentiostat/Galvanostat using a standard three-electrode configuration. The working electrode was the basal plane of highly oriented pyrolytic graphite (HOPG) (GraphiteStore.com, Buffalo Grove, Ill.; surface area: 0.09 cm^2), the counter electrode was a platinum wire (Kurt J. Lesker, Jefferson Hills, PA; 99.99%, 0.5 mm diameter), and a silver wire immersed in electrolyte served as a pseudo-reference electrode (CH Instruments). The reference was separated from the working solution by a Vycor frit (Bioanalytical Systems, Inc.). Ferrocene (Sigma Aldrich; twice-sublimed) was added to the electrolyte solution at the conclusion of each experiment (~1 mM); the midpoint potential of the ferrocenium/ferrocene couple (denoted as $Fc^{+/0}$) served as an external standard for comparison of the recorded potentials. Concentrations of analyte for cyclic voltammetry were typically 1 mM.

Synthetic Procedures. Ligands were synthesized by modification of related procedures from the literature.[27,28]

Synthesis of **LBn$_2$.** A Schlenk flask with bis(2-pyridyl)methane (dpma; 0.6509 g, 3.82 mmol, 1.0 equiv.) was cooled to –78°C. A solution of nBuLi (1.67 mL, 4.59 mmol, 1.2 equiv.) was added dropwise and allowed to stir for 15 min then benzyl bromide (0.59 mL, 4.47 mmol, 1.3 equiv.) was added dropwise. The sequential addition of nBuLi (1.95 mL, 5.35 mmol, 1.4 equiv.) and benzyl bromide (0.68 mL, 5.74 mmol, 1.5 equiv.) was then repeated in the same manner. The resulting yellow solution was stirred with a saturated solution of sodium bicarbonate. The liquid phase was separated by filtration and title ligand was then purified and obtained by a dichloromethane/water separation followed by a column with 50:50 dichloromethane:acetone column. (0.9889 g, 74% yield). ^1H NMR (500 MHz, C_6D_6): δ 8.51 – 8.46 (m, 2H), 6.99 – 6.93 (m, 7H), 6.90 – 6.80 (m, 7H), 6.69 (dd, *J* = 8.1, 1.2 Hz, 2H), 6.58 (ddd, J = 7.5, 4.8, 1.1 Hz, 2H), 4.01 (s, 4H) ppm. $^{13}C\{^1H\}$ NMR (126 MHz, C_6D_6): δ 165.26 (d, *J* = 5.2 Hz), 148.39 (d, *J* = 5.1 Hz), 139.47 (d, *J* = 5.2 Hz), 135.01 (d, *J* = 5.3 Hz), 131.21 (d, *J* = 5.3 Hz), 128.37, 127.77 (d, *J* = 5.1 Hz) 126.14 (d, *J* = 5.4 Hz), 124.75 (d, *J* = 5.4 Hz), 121.11 (d, *J* = 5.4 Hz), 59.21 (d, *J* = 5.3 Hz), 44.68 (d, *J* = 5.3 Hz) ppm.

Synthesis of **LMePyr.** A solution of tBuOK in THF (0.3005 g, 2.67 mmol, 1.2 equiv.) was added dropwise to a Schlenk flask charged with 2,2′-(ethane-1,1-diyl)dipyridine (0.4111 g, 2.23 mmol, 1.0 equiv.) at –78°C. The solution was stirred for 45 min and turned a light peach color. A solution of 1-chloromethylpyrene in THF (0.7274 g, 2.90 mmol, 1.3 equiv.) was added to the Schlenk, which was then allowed to warm to room temperature and refluxed overnight. Following reflux, the solution was cooled then stirred with a saturated solution of sodium bicarbonate and the liquid phase separated by filtration. Purification was accomplished by extraction of the product mixture with dichloromethane/water followed by column chromatography with chloroform as the initial eluent. However, the desired ligand was finally eluted from the column with methanol (0.4559 g, 51% yield). ^1H NMR (500 MHz, CD_2Cl_2): δ 8.66 – 8.61 (m, 2H), 8.25 – 8.09 (m, 3H), 8.06 – 7.90 (m, 4H), 7.85 (d, *J* = 7.9 Hz, 1H), 7.52 (td, *J* = 7.8, 1.9 Hz, 2H), 7.21 – 7.12 (m, 3H), 7.02 (dd, *J* = 8.0, 1.1 Hz, 2H), 4.56 (s, 2H), 1.64 (s, 3H) ppm. $^{13}C\{^1H\}$ NMR (126 MHz, CD_2Cl_2): δ 167.46, 149.12, 136.44, 134.38, 131.89, 131.27, 131.09, 130.27, 129.87, 127.94, 127.19, 126.99, 126.26, 125.32, 125.23, 125.04, 125.00, 124.42, 123.06, 121.75, 41.80, 25.87 ppm.

Synthesis of **LPyr$_2$.** A solution of tBuOK in THF (0.8587 g, 7.65 mmol, 2.5 equiv.) was added dropwise to a Schlenk flask charged with bis(2-pyridyl)methane (dpma; 0.5211 g, 3.06 mmol, 1 equiv.) at –78°C. The solution was stirred for 45 min and turned a light peach color. A solution of 1-chloromethylpyrene in THF (0.1.9952 g, 7.95 mmol, 2.6 equiv.) was added to the Schlenk then warmed to room temperature and refluxed overnight. Following reflux, the solution was first allowed to cool and then a stirred with a saturated solution of sodium bicarbonate; the liquid phase was then separated by filtration. The liquid phase was then extracted with dichloromethane/water and subjected to column chromatography with chloroform as the eluent. The desired ligand was eluted from the column with methanol (0.5504 g, 30% yield). ^1H NMR (500 MHz, $CDCl_3$): δ 8.71 (s, 2H), 8.10 (dd, *J* = 7.6, 1.2 Hz, 2H), 8.02 (d, *J* = 7.3 Hz, 2H), 7.99 – 7.89 (m, 7H), 7.86 (d, *J* = 8.0 Hz, 3H), 7.75 (d, *J* = 8.0 Hz, 2H), 7.70 (d, *J* = 9.4 Hz, 2H), 6.99 (s, 4H), 6.54 (s, 2H), 4.74 (s, 4H) ppm. $^{13}C\{^1H\}$ NMR (126 MHz, CD_3CN): δ 146.97, 131.35, 130.82, 130.69, 130.57, 130.23, 128.77, 127.43, 127.27, 125.96 (d, *J* = 4.2 Hz), 125.13, 124.98, 124.71 (d, *J* = 2.5 Hz), 124.20, 123.25, 100.12, 41.53 ppm.

Synthesis of **A^{LBn2}.** To a suspension of $[Cp^*RhCl_2]_2$ in CH_3CN (0.1717 g, 0.278 mmol, 0.5 equiv.) were added $AgPF_6$ (0.1405 g, 0.556 mmol, 1.0 equiv.) in CH_3CN and **L^{Bn2}** ligand (0.1947 g, 0.556 mmol, 1.05 etriquiv.) as a THF solution. The reaction mixture rapidly changed from brick red to orange, and a yellowish precipitate formed. After 15 min, the suspension was filtered to remove the AgCl byproduct, and the volume of the filtrate was reduced to ~1 mL. Addition of Et_2O (~80 mL) caused precipitation of a yellow solid, which was collected by filtration. Pure material was obtained via recrystallization with vapor diffusion of Et_2O into a concentrated CH_3CN solution of the title compound (0.1581 g, 37%). Vapor diffusion of Et_2O into

a smaller concentrated CH_3CN solution was employed to obtain single crystals suitable for X-ray diffraction studies. ^{1}H NMR (500 MHz, CD_3CN): δ 9.00 (dd, *J* = 5.8, 1.7 Hz, 2H), 7.73 (ddd, *J* = 8.3, 7.4, 1.8 Hz, 2H), 7.52 (ddd, *J* = 7.4, 5.7, 1.4 Hz, 2H), 8.37 (d, *J* = 8.3 Hz, 2H), 7.35 – 7.16 (m, 4H), 7.03 – 6.99 (m, 4H), 6.60 – 6.50 (m, 2H), 6.49 – 6.44 (m, 2H), 3.85 (s, 2H), 3.67 (s, 2H), 1.59 (s, 15H) ppm. ^{13}C{^{1}H} NMR (126 MHz, CD_3CN): δ 161.15, 159.57, 157.97, 140.25, 139.11, 136.30, 135.26, 131.55, 131.32, 130.78, 129.34, 128.84, 128.58, 128.34, 128.01, 126.89, 126.77, 126.12, 125.28, 124.95, 99.14, 55.79, 49.06, 40.75, 9.55 ppm. ^{19}F NMR (376 MHz, CD_3CN): δ −73.80 (d, $^1J_{F,P}$ = 706 Hz) ppm. ^{31}P{^{1}H} NMR (162 MHz, CD_3CN): δ −145.50 (sept, $^1J_{P,F}$ = 706 Hz) ppm. Anal. Calcd for $C_{35}H_{37}ClF_6N_2PRh$: C, 54.67; H, 4.85, N, 3.64. Found: C, 54.70; H, 4.88, N, 4.97. Calcd for $C_{35}H_{37}ClF_6N_2PRh$ + 1CH_3CN: C, 54.86; H, 4.98, N, 5.19. This analysis is consistent with observation of CH_3CN in the ^{1}H NMR spectra for $\mathbf{A}^{\mathbf{LBn2}}$ (see SI).

Synthesis of $\mathbf{A}^{\mathbf{LMePyr}}$**.** To a suspension of $[Cp^*RhCl_2]_2$ in CH_3CN (0.0999 g, 0.162. mmol, 0.5 equiv.) were added $AgPF_6$ (0.0817 g, 0.323 mmol, 1.0 equiv.) in CH_3CN and $\mathbf{L}^{\mathbf{MePyr}}$ ligand (0.1320 g, 0.331 mmol, 1.05 equiv.) as a THF solution. The reaction mixture rapidly changed from brick red to orange, and a yellowish precipitate formed. After 15 min, the suspension was filtered to remove the AgCl byproduct, and the volume of the filtrate was reduced to ~1 mL. Addition of Et_2O (~80 mL) caused precipitation of a yellow solid, which was collected by filtration. Pure material was obtained via crystallization by vapor diffusion of Et_2O into a concentrated CH_2Cl_2 solution of the title compound (0.080 g, 30%). The same method was employed to obtain single crystals suitable for X-ray diffraction studies. ^{1}H NMR (500 MHz, CD_3CN): δ 9.05 (bs, 2H), 8.29 (d, *J* = 1.04 Hz, 3H), 8.23 – 8.12 (m, 5H), 8.12 – 8.05 (m, 3H), 7.93 (d, *J* = 7.9 Hz, 2H), 7.61 (t, *J* = 6.8 Hz, 2H), 6.52 (d, *J* = 7.9 Hz, 2H), 5.02 (broad s, 1H), 4.14 (broad s, 1H), 1.73 (s, 3H), 1.68 (s, 15H) ppm. ^{13}C{^{1}H} NMR (126 MHz, CD_3CN): δ 158.48, 141.44, 141.12, 132.29, 131.58, 131.44, 128.68, 128.54, 128.20, 128.03, 127.46, 126.52, 126.13, 125.82, 125.33, 124.62, 124.56, 99.20, 99.18, 52.26, 40.45, 23.81, 9.59 ppm. ^{19}F NMR (376 MHz, CD_3CN): δ −73.83 (d, $^1J_{F,P}$ = 706 Hz) ppm. ^{31}P{^{1}H} NMR (162 MHz, CD_3CN): δ −145.51 (sept, $^1J_{P,F}$ = 706 Hz) ppm. Satisfactory elemental analysis could not be obtained for $\mathbf{A}^{\mathbf{LMePyr}}$, but NMR methods confirm the diamagnetic purity of the isolated material.

Synthesis of $\mathbf{A}^{\mathbf{LPyr2}}$**.** To a suspension of $[Cp^*RhCl_2]_2$ in CH_3CN (0.0399 g, 0.0646 mmol, 0.5 equiv.) were added $AgPF_6$ (0.0326 g, 0.129 mmol, 1.0 equiv.) in CH_3CN and $\mathbf{L}^{\mathbf{Pyr2}}$ ligand (0.0793 g, 0.132 mmol, 1.05 equiv.) as a THF solution. The reaction mixture rapidly changed from brick red to orange, and a yellowish precipitate formed. After 15 min, the suspension was filtered to remove the AgCl byproduct, and the volume of the filtrate was reduced to ~1 mL. Addition of Et_2O (~80 mL) caused precipitation of a yellow solid, which was collected by filtration. Pure material was obtained via crystallization by vapor diffusion of Et_2O into a concentrated CH_2Cl_2 solution of the title compound (0.0250 g, 26%). Vapor diffusion of Et_2O into a smaller concentrated CH_2Cl_2 solution was employed to obtain single crystals suitable for X-ray diffraction studies. ^{1}H NMR (500 MHz, CD_3CN): δ 9.16 (s, 2H), 8.74 (d, *J* = 9.3 Hz, 1H), 8.51 (dd, *J* = 8.5, 4.7 Hz, 2H), 8.37 (d, *J* = 7.6 Hz, 1H), 8.28 – 8.07 (m, 7H), 8.04 – 7.93 (m, 4H), 7.85 (dd, *J* = 13.6, 9.1 Hz, 3H), 7.74 (d, *J* = 9.3 Hz, 1H), 7.59 (d, *J* = 5.8 Hz, 3H), 7.54 (d, *J* = 8.1 Hz, 2H), 6.59 (d, *J* = 8.0 Hz, 1H), 6.28 (d, *J* = 8.1 Hz, 1H), 4.66 (s, 2H), 1.73 (s, 15H) ppm. ^{13}C{^{1}H} NMR (126 MHz, CD_3CN): δ 158.32, 140.34, 132.36, 132.13, 132.00, 131.91, 131.74, 131.34, 130.47, 130.43, 129.73, 129.27, 129.18, 129.11, 129.05, 128.82, 128.34, 128.29, 128.17, 127.94, 127.63, 127.29, 126.84, 126.57, 126.45, 126.39, 126.33, 126.02, 125.50, 125.32, 125.28, 124.84, 124.81, 123.96, 123.38, 99.37, 99.31, 57.27, 44.96, 39.08, 9.63. ppm. ^{19}F NMR (376 MHz, CD_3CN): δ −74.77 (d, $^1J_{F,P}$ = 706 Hz) ppm. ^{31}P{^{1}H} NMR (162 MHz, CD_3CN): δ −144.65 (sept, $^1J_{P,F}$ = 706 Hz) ppm. Anal. Calcd for $C_{55}H_{45}ClF_6N_2PRh$: C, 64.94; H, 4.46, N, 2.75. Found: C, 61.50; H, 4.65, N, 2.45. Calcd for $C_{55}H_{45}ClF_6N_2PRh$ + 1CH_2Cl_2: C, 61.02; H, 4.80, N, 2.61. This analysis is consistent with the single co-crystallized CH_2Cl_2 solvent molecule found in the solid-state structure of $\mathbf{A}^{\mathbf{LPyr2}}$ (see SI).

Synthesis of $\mathbf{1}^{\mathbf{LBn2}}$**.** To an orange solution of $\mathbf{A}^{\mathbf{LBn2}}$ in CH_3CN (0.0508 g, 0.064 mmol) was added $AgPF_6$ (0.0167 g, 0.066 mmol, 1 equiv.) in CH_3CN. The solution lightened to a pale-yellow color, and a colorless precipitate formed. The mixture was stirred for 3 hours; it was then filtered through Celite to remove AgCl and the volatiles removed *in vacuo*. $\mathbf{1}^{\mathbf{LBn2}}$ ^{1}H NMR (500 MHz, CD_3CN): δ 8.99 (dd, *J* = 5.9, 1.7 Hz, 2H), 8.01 – 7.87 (m, 2H), 7.79 – 7.61 (m, 4H), 7.36 – 7.24 (m, 4H), 7.11 – 6.99 (m, 4H), 6.60 (d, *J* = 7.1 Hz, 2H), 6.44 (d, *J* = 7.3 Hz, 2H), 3.83 (s, 2H), 3.59 (s, 2H), 1.60 (s, 15H) ppm.

Synthesis of $\mathbf{1}^{\mathbf{LMePyr}}$**.** To an orange solution of $\mathbf{A}^{\mathbf{LMePyr}}$ in CH_3CN (0.0462 g, 0.047 mmol) was added $AgPF_6$ (0.0119 g, 0.443 mmol, 1 equiv.) in CH_3CN. The solution lightened to a pale-yellow color, and a colorless precipitate formed. The mixture was stirred for 3 hours; it was then filtered through Celite to remove AgCl and the volatiles removed *in vacuo*. $\mathbf{1}^{\mathbf{LMePyr}}$ ^{1}H NMR (500 MHz, CD_3CN): δ 9.16 (s, 2H), 8.76 (d, *J* = 9.3 Hz, 1H), 8.53 (t, *J* = 8.1 Hz, 2H), 8.39 (d, *J* = 7.6 Hz, 1H), 8.28 – 8.17 (m, 4H), 8.15 – 8.07 (m, 2H), 8.05 – 7.96 (m, 4H), 7.87 (dd, *J* = 17.0, 9.2 Hz, 3H), 7.79 – 7.71 (m, 4H), 7.67 (d, *J* = 9.3 Hz, 1H), 7.59 (d, J = 8.1 Hz, 2H), 6.46 (d, *J* = 8.0 Hz, 1H), 6.40 (d, *J* = 8.2 Hz, 1H), 4.50 (s, 2H), 1.78 (s, 15H) ppm.

Synthesis of $\mathbf{1}^{\mathbf{LPyr2}}$**.** To an orange solution of $\mathbf{A}^{\mathbf{LPyr2}}$ in CH_3CN (0.0532 g, 0.053 mmol) was added $AgPF_6$ (0.0132 g, 0.052 mmol, 1 equiv.) in CH_3CN. The solution lightened to a pale-yellow color, and a colorless precipitate formed. The mixture was stirred for 3 hours; it was then filtered through Celite to remove AgCl and the volatiles removed *in vacuo*. $\mathbf{1}^{\mathbf{LPyr2}}$ ^{1}H NMR (500 MHz, CD_3CN): δ 9.02 (broad s, 2H), 8.34 – 8.27 (m, 2H), 8.20 (d, *J* = 2.8 Hz, 2H), 8.17 (s, 1H), 8.15 (s, 1H), 8.13 – 8.06 (m, 4H), 7.93 (d, *J* = 8.0 Hz, 1H), 7.76 (t, *J* = 6.7 Hz, 3H), 6.45 (d, *J* = 8.0 Hz, 1H), 4.55 (broad s, 1H), 4.18 (broad s, 1H), 1.73 (s, 15H), 1.68 (s, 3H) ppm.

Synthesis of $\mathbf{4}^{\mathbf{LBn2}}$**.** A suspension of $\mathbf{A}^{\mathbf{LBn2}}$ in THF (0.0698 g, 0.0759 mmol) was stirred over freshly prepared sodium-mercury amalgam (1% Na in Hg; 0.0175 g Na^0, 0.759 mmol, 10 equiv.) for 6 hours, during which time the yellow suspension became a dark red homogeneous solution. The mixture was filtered, and the volatiles removed in vacuo. Extraction with Et_2O and removal of the volatiles in vacuo provides the title compound as a dark red solid (0.0349 g, 77%). Extraction with hexanes can provide additional pure material, if the extracted solution is cooled to −35°C; these conditions provide additional pure and crystalline product. This strategy was employed using pure material to obtain single-crystals of the title compound suitable for X-ray diffraction studies. ^{1}H NMR (400 MHz, C_6D_6) δ 8.42 (dd, *J* = 3.5, 1.8 Hz, 1H), 8.33 (d, *J* = 5.5 Hz, 1H), 7.10 – 7.02 (m, 4H), 6.93 – 6.83 (m, 3H), 6.74 – 6.68 (m, 2H), 6.57 (td, *J* = 7.7, 1.6 Hz, 1H), 6.51 (dd, *J* = 7.7, 1.9 Hz, 2H), 6.24 (d, *J* = 7.9 Hz, 1H), 6.17 (ddd, *J* = 7.2, 5.6, 1.4 Hz, 1H), 6.10 (dd, *J* = 8.5, 3.5 Hz, 1H), 4.85 (d, *J* = 13.4 Hz, 1H), 4.23 (d, *J* = 13.4 Hz, 1H), 3.38 (d, *J* = 13.7 Hz, 1H), 3.04 (d, *J* = 13.6 Hz, 1H), 1.50 (s, 15H). ^{13}C NMR (126 MHz, C_6D_6) δ 165.03, 151.77, 146.11, 145.17, 140.43, 139.16, 131.82, 131.10, 127.37, 126.17, 125.86, 125.67, 121.32, 111.63, 91.23 (d, *J* = 5.5 Hz), 88.55 (d, *J* = 16.9 Hz), 65.64, 53.03 (d, *J* = 12.7 Hz), 46.83, 41.89, 9.01 ppm. $\mathbf{4}^{\mathbf{LBn2}}$ is acutely air sensitive and satisfactory elemental analysis results could not be obtained.

ASSOCIATED CONTENT

Supporting Information

The Supporting Information is available free of charge on the ACS Publications website.

NMR spectra and characterization of complexes and additional electrochemical, simulations, reactivity, and X-ray crystallographic data (PDF)

Cartesian coordinates (XYZ)

Accession Codes

CCDC entries 2041687, 2033846, 2033845, 2033848 contain the supplementary crystallographic data for select compounds reported in this paper. These data can be obtained free of charge via www.ccdc.cam.ac.uk/data_request/cif, or by emailing data_request@ccdc.cam.ac.uk, or by contacting The Cambridge Crystallographic Data Centre, 12 Union Road, Cambridge CB2 1EZ, UK; fax: +44 1223 336033.

AUTHOR INFORMATION

Corresponding Author

* To whom correspondence should be addressed. E-mail: blakemore@ku.edu, phone: +1 (785) 864-3019 (J.D.B.)

ORCID

James D. Blakemore: 0000-0003-4172-7460
Julie A. Leseberg: 0000-0001-6895-7333

Notes

Present Address:
[†] Department of Chemistry, Franklin & Marshall College, P.O. Box 3003, Lancaster, Pennsylvania, United States.

The authors declare no competing financial interest.

ACKNOWLEDGMENT

The authors thank Dr. Justin Douglas and Sarah Neuenswander for assistance with NMR spectroscopy. This work was supported by the US National Science Foundation through award OIA-1833087. Support for NMR instrumentation was provided by NIH Shared Instrumentation Grants S10OD016360 and S10RR024664 and by the NSF MRI grant CHE-1625923.

REFERENCES

[1] Lewis, N. S.; Nocera, D. G., Powering the planet: Chemical challenges in solar energy utilization. *Proc. Nat. Acad. Sci. U.S.A.* **2006**, *103*, 15729-15735.

[2] (a) Rakowski Dubois, M.; Dubois, D. L., Development of Molecular Electrocatalysts for CO2 Reduction and H2 Production/Oxidation. *Acc. Chem. Res.* **2009**, *42*, 1974-1982. (b) Qiao, J.; Liu, Y.; Hong, F.; Zhang, J., A review of catalysts for the electroreduction of carbon dioxide to produce low-carbon fuels. *Chem. Soc. Rev.* **2014**, *43*, 631-675.

[3] Gassman, P. G.; Macomber, D. W.; Willging, S. M., Isolation and characterization of reactive intermediates and active catalysts in homogeneous catalysis. *J. Am. Chem. Soc.* **1985**, *107*, 2380-2388.

[4] (a) Sconyers, D. J.; Blakemore, J. D., Distinguishing between homogeneous and heterogeneous hydrogen-evolution catalysis with molecular cobalt complexes. *Chem. Commun.* **2017**, *53*, 7286-7289. (b) Kumar, A.; Lionetti, D.; Day, V. W.; Blakemore, J. D., Redox-Inactive Metal Cations Modulate the Reduction Potential of the Uranyl Ion in Macrocyclic Complexes. *J. Am. Chem. Soc.* **2020**, *142*, 3032-3041.

[5] (a) Costentin, C.; Savéant, J.-M., Concepts and tools for mechanism and selectivity analysis in synthetic organic electrochemistry. *Proc Natl Acad Sci U S A* **2019**, *116*, 11147-11152. (b) Lexa, D.; Sayeant, J. M.; Zickler, J., Electrochemistry of vitamin B12. 5. Cyanocobalamins. *J. Am. Chem. Soc.* **1980**, *102*, 2654-2663. (c) Grass, V.; Lexa, D.; Momenteau, M.; Savéant, J.-M., Reductive Electrochemistry of Rhodium Porphyrins. Disproportionation of Intermediary Oxidation States. *J. Am. Chem. Soc.* **1997**, *119*, 3536-3542. (d) Amatore, C.; Gareil, M.; Savéant, J. M., Homogeneous vs. heterogeneous electron transfer in electrochemical reactions: Application to the electrohydrogenation of anthracene and related reactions. *J. Electroanal. Chem. Interfacial Electrochem.* **1983**, *147*, 1-38.

[6] (a) Boyd, E. A.; Lionetti, D.; Henke, W. C.; Day, V. W.; Blakemore, J. D., Preparation, Characterization, and Electrochemical Activation of a Model [Cp*Rh] Hydride. *Inorg. Chem.* **2018**, *58*, 3606-3615. (b) Hopkins, J. A.; Lionetti, D.; Day, V. W.; Blakemore, J. D., Chemical and Electrochemical Properties of [Cp*Rh] Complexes Supported by a Hybrid Phosphine-Imine Ligand. *Organometallics* **2019**, *38*, 1300-1310.

[7] (a) Ward, M. D.; McCleverty, J. A., Non-innocent behaviour in mononuclear and polynuclear complexes: consequences for redox and electronic spectroscopic properties. *J. Chem. Soc., Dalton Trans.* **2002**, 275-288. (b) Chirik, P. J.; Wieghardt, K., Radical Ligands Confer Nobility on Base-Metal Catalysts. *Science* **2010**, *327*, 794-795. (c) Kaim, W.; Schwederski, B., Non-innocent ligands in bioinorganic chemistry—An overview. *Coord. Chem. Rev.* **2010**, *254*, 1580-1588. (d) Lyaskovskyy, V.; de Bruin, B., Redox Non-Innocent Ligands: Versatile New Tools to Control Catalytic Reactions. *ACS Catalysis* **2012**, *2*, 270-279. (e) Berben, L. A.; de Bruin, B.; Heyduk, A. F., Non-innocent ligands. *Chem. Commun.* **2015**, *51*, 1553-1554. (f) Zell, T.; Milstein, D., Hydrogenation and Dehydrogenation Iron Pincer Catalysts Capable of Metal–Ligand Cooperation by Aromatization/Dearomatization. *Acc. Chem. Res.* **2015**, *48*, 1979-1994.

[8] (a) Kaes, C.; Katz, A.; Hosseini, M. W., Bipyridine: The Most Widely Used Ligand. A Review of Molecules Comprising at Least Two 2,2′-Bipyridine Units. *Chem. Rev.* **2000**, *100*, 3553-3590. (b) Kölle, U.; Grätzel, M., Metallorganische Rhodium(III)-Komplexe als Homogenkatalysatoren für die Photoreduktion von Protonen zu Wasserstoff an kolloidalem TiO_2. *Angew. Chem.* **1987**, *99*, *572–574*. (c) Kölle, U.; Grätzel, M., Organometallic Rhodium(III) Complexes as Catalysts for the Photoreduction of Protons to Hydrogen on Colloidal TiO_2. *Angew. Chem. Int.* Ed. Engl. **1987**, *26*, *567 –570*. (d) Wang, W.-H.; Hull, J. F.; Muckerman, J. T.; Fujita, E.; Himeda, Y., Second-coordination-sphere and electronic effects enhance iridium(iii)-catalyzed homogeneous hydrogenation of carbon dioxide in water near ambient temperature and pressure. *Energy Environ. Sci.* **2012**, *5*, 7923-7926. (e) Chardon-Noblat, S.; Cosnier, S.; Deronzier, A.; Vlachopoulos, N., Electrochemical properties of $[(C_5Me_5)Rh^{III}(L)Cl]^+$ complexes (L = 2,2′-bipyridine or 1,10-phenanthroline derivatives) in solution in related polypyrrolic films. Application to electrocatalytic hydrogen generation. *J. Electroanal. Chem.* **1993**, *352*, 213-228. (f) Caix, C.; Chardon-Noblat, S.; Deronzier, A.; Moutet, J.-C.; Tingry, S., (Pentamethylcyclopentadienyl)(polypyridyl) rhodium and iridium complexes as electrocatalysts for the reduction of protons to dihydrogen and the hydrogenation of organics. *J. Organomet. Chem.* **1997**, *540*, 105-111. (g) Blakemore, J. D.; Gupta, A.; Warren, J. J.; Brunschwig, B. S.; Gray, H. B., Noncovalent Immobilization of Electrocatalysts on Carbon Electrodes for Fuel Production. *J. Am. Chem. Soc.* **2013**, *135*, 18288-18291. (h) Brintzinger, H.; Bercaw, J. E., Bis(pentamethylcyclopentadienyl)titanium(II). Isolation and reactions with hydrogen, nitrogen, and carbon monoxide. *J. Am. Chem. Soc.* **1971**, *93*, 2045-2046.

[9] (a) Gibson, V. C.; Redshaw, C.; Solan, G. A., Bis(imino)pyridines: Surprisingly Reactive Ligands and a Gateway to New Families of Catalysts. *Chem. Rev.* **2007**, *107*, 1745-1776. (b) Small, B. L.; Brookhart, M., Iron-Based Catalysts with Exceptionally High Activities and Selectivities for Oligomerization of Ethylene to Linear α-Olefins. *J. Am. Chem. Soc.* **1998**, *120*,

7143-7144. (c) Bennett, A. M. A. Iron catalyst for the polymerization of olefins. US 6214761 B1, 2001. (d) J. P. Britovsek, G.; C. Gibson, V.; J. McTavish, S.; A. Solan, G.; J. P. White, A.; J. Williams, D.; J. P. Britovsek, G.; S. Kimberley, B.; J. Maddox, P., Novel olefin polymerization catalysts based on iron and cobalt. *Chem. Commun.* **1998**, 849-850. (e) Small, B. L., Discovery and Development of Pyridine-bis(imine) and Related Catalysts for Olefin Polymerization and Oligomerization. *Acc. Chem. Res.* **2015**, *48*, 2599-2611. (f) Chirik, P. J., Iron- and Cobalt-Catalyzed Alkene Hydrogenation: Catalysis with Both Redox-Active and Strong Field Ligands. *Acc. Chem. Res.* **2015**, *48*, 1687-1695. (g) Chirik, P. J., Carbon–Carbon Bond Formation in a Weak Ligand Field: Leveraging Open-Shell First-Row Transition-Metal Catalysts. *Angew. Chem. Int. Ed.* **2017**, *56*, 5170-5181.(h) Obligacion, J. V.; Chirik, P. J., Earth-abundant transition metal catalysts for alkene hydrosilylation and hydroboration. *Nature Reviews Chemistry* **2018**, *2*, 15-34.(i) Trovitch, R. J., The Emergence of Manganese-Based Carbonyl Hydrosilylation Catalysts. *Acc. Chem. Res.* **2017**, *50*, 2842-2852. (j) Nückel, S.; Burger, P., Transition-Metal Complexes with Sterically Demanding Ligands: Facile Thermal Intermolecular C•H Bond Activation in a Square-Planar Ir^{I} Complex. *Angew. Chem. Int. Ed.* **2003**, *42*, 1632-1636. (k) Tang, J.; Gamez, P.; Reedijk, J., Efficient [bis(imino)pyridine-iron]-catalyzed oxidation of alkanes. *Dalton Trans.* **2007**, 4644-4646. (l) Britovsek, G. J. P.; England, J.; Spitzmesser, S. K.; White, A. J. P.; Williams, D. J., Synthesis of iron(ii), manganese(ii) cobalt(ii) and ruthenium(ii) complexes containing tridentate nitrogen ligands and their application in the catalytic oxidation of alkanes. *Dalton Trans.* **2005**, 945-955. (m) Cui, P.; Wang, Q.; McCollom, S. P.; Manor, B. C.; Carroll, P. J.; Tomson, N. C., Ring-Size-Modulated Reactivity of Putative Dicobalt-Bridging Nitrides: C−H Activation versus Phosphinimide Formation. *Angew. Chem. Int. Ed.* **2017**, *56*, 15979-15983. (n) Bart, S. C.; Lobkovsky, E.; Chirik, P. J., Preparation and Molecular and Electronic Structures of Iron(0) Dinitrogen and Silane Complexes and Their Application to Catalytic Hydrogenation and Hydrosilation. *J. Am. Chem. Soc.* **2004**, *126*, 13794-13807. (o) Margulieux, G. W.; Bezdek, M. J.; Turner, Z. R.; Chirik, P. J., Ammonia Activation, H_2 Evolution and Nitride Formation from a Molybdenum Complex with a Chemically and Redox Noninnocent Ligand *J. Am. Chem. Soc.* **2017**, *139*, 6110-6113. (p) Manuel, T. D.; Rohde, J.-U., Reaction of a Redox-Active Ligand Complex of Nickel with Dioxygen Probes Ligand-Radical Character. *J. Am. Chem. Soc.* **2009**, *131*, 15582-15583. (q) Badiei, Y. M.; Siegler, M. A.; Goldberg, D. P., O_2 Activation by Bis(imino)pyridine Iron(II)−Thiolate Complexes. *J. Am. Chem. Soc.* **2011**, *133*, 1274-1277. (r) Lau, K.-C.; Jordan, R. F., Reactivity of (Pyridine-Diimine)Fe Alkyl Complexes with Carbon Dioxide. *Organometallics* **2016**, *35*, 3658-3666. (s) Rummelt, S. M.; Zhong, H.; Korobkov, I.; Chirik, P. J., Iron-Mediated Coupling of Carbon Dioxide and Ethylene: Macrocyclic Metallalactones Enable Access to Various Carboxylates. *J. Am. Chem. Soc.* **2018**, *140*, 11589-11593.

[10] Bezdek, M. J.; Chirik, P. J., Pyridine(diimine) Chelate Hydrogenation in a Molybdenum Nitrido Ethylene Complex. *Organometallics* **2019**, *38*, 1682-1687.

[11] (a) Chirik, P. J.; Wieghardt, K., Radical Ligands Confer Nobility on Base-Metal Catalysts. *Science* **2010**, *327*, 794-795. (b) Chirik, P. J., Preface: Forum on Redox-Active Ligands. *Inorg. Chem.* **2011**, *50*, 9737-9740. (e) Römelt, C.; Weyhermüller, T.; Wieghardt, K., Structural characteristics of redox-active pyridine-1,6-diimine complexes: Electronic structures and ligand oxidation levels. *Coord. Chem. Rev.* **2019**, *380*, 287-317.

[12] Kaim, W.; Reinhardt, R.; Waldhör, E.; Fiedler, J., Electron transfer and chloride ligand dissociation in complexes $[(C_5Me_5)Cl\,M(bpy)]^{+}/[(C_5Me_5)M(bpy)]^{n}$ (M=Co, Rh, Ir; n = 2+, +, 0, −): A combined electrochemical and spectroscopic investigation. *J. Organomet. Chem.* **1996**, *524*, 195-202.

[13] Lionetti, D.; Day, V. W.; Blakemore, J. D., Synthesis and Electrochemical Properties of Half-Sandwich Rhodium and Iridium Methyl Complexes. *Organometallics* **2017**, *36*, 1897-1905.

[14] (a) Gore-Randall, E.; Irwin, M.; Denning, M. S.; Goicoechea, J. M., Synthesis and Characterization of Alkali-Metal Salts of 2,2′- and 2,4′-Bipyridyl Radicals and Dianions. *Inorg. Chem.* **2009**, *48*, 8304-8316. (b) Dallinger, R. F.; Woodruff, W. H., Time-resolved resonance Raman study of the lowest (d.pi.*,3CT) excited state of tris(2,2'-bipyridine)ruthenium(II). *J. Am. Chem. Soc.* **1979**, *101*, 4391-4393. (c) Creutz, C., Bipyridine radical ions. *Comments Inorg. Chem.* **1982,** *1*, 293-311.

[15] Lionetti, D.; Day, V. W.; Lassalle-Kaiser, B.; Blakemore, J. D., Multiple binding modes of an unconjugated bis(pyridine) ligand stabilize low-valent [Cp*Rh] complexes. *Chem. Commun.* **2018**, 54, 1694-1697.

[16] (a) Nakai, H.; Jeong, K.; Matsumoto, T.; Ogo, S., Catalytic C–F Bond Hydrogenolysis of Fluoroaromatics by $[(\eta^5\text{-}C_5Me_5)RhI(2,2'\text{-bipyridine})]$. *Organometallics* **2014**, *33*, 4349-4352. (b) Blakemore, J. D.; Hernandez, E. S.; Sattler, W.; Hunter, B. M.; Henling, L. M.; Brunschwig, B. S.; Gray, H. B., Pentamethylcyclopentadienyl rhodium complexes. *Polyhedron* **2014**, *84*, 14-18. (c) Lionetti, D.; Day, V. W.; Blakemore, J. D., Synthesis and Electrochemical Properties of Half-Sandwich Rhodium and Iridium Methyl Complexes. *Organometallics* **2017**, *36*, 1897-1905.

[17] (a) Dewar, M. J. S.; Ford, G. P., Relationship between olefinic .pi. complexes and three-membered rings. *J. Am. Chem. Soc.* **1979**, *101*, 783-791. (b) Chatt, J.; Duncanson, L. A., Olefin coordination compounds. Part III. Infra-red spectra and structure: attempted preparation of acetylene complexes. *J. Chem. Soc.* **1953**, 2939-2947.

[18] Nicholson, R. S.; Shain, I., Theory of Stationary Electrode Polarography. Single Scan and Cyclic Methods Applied to Reversible, Irreversible, and Kinetic Systems. *Anal. Chem.* **1964**, *36*, 706-723.

[19] Saveant, J. *Elements of Molecular and Biomolecular Electrochemistry,* 1st ed.; Wiley, 2006.

[20] Lionetti, D.; Day, V. W.; Blakemore, J. D., Structural and chemical properties of half-sandwich rhodium complexes supported by the bis(2-pyridyl)methane ligand. *Dalton Trans.* **2019**, *48*, 12396-12406.

[21] (a) Sommerfeld, N. S.; Gülzow, J.; Roller, A.; Cseh, K.; Jakupec, M. A.; Grohmann, A.; Galanski, M.; Keppler, B. K., Antiproliferative Copper(II) and Platinum(II) Complexes with Bidentate N,N-Donor Ligands. *Chem. Eur. J.* **2017**, *2017*, 3115-3124. (b) Elie, M.; Weber, M. D.; Di Meo, F.; Sguerra, F.; Lohier, J.-F.; Pansu, R. B.; Renaud, J.-L.; Hamel, M.; Linares, M.; Costa, R. D.; Gail-lard, S., Role of the Bridging Group in Bis-Pyridyl Ligands: Enhancing Both the Photo- and Electroluminescent Features of Cationic (IPr)CuI Complexes. *Chem. Eur. J.* **2017**, *23*, 16328-16337. (c) Mohr, F.; Binfield, S. A.; Fettinger, J. C.; Vedernikov, A. N., A Practical, Fast, and High-Yielding Aziridination Procedure Using Simple Cu(II)

Complexes Containing N-Donor Pyridine-Based Ligands. *J. Org. Chem.* **2005**, *70*, 4833-4839.

[22] Canty, A. J.; Chaichit, N.; Gatehouse, B. M.; George, E. E.; Hayhurst, G., Coordination chemistry of methylmercury(II). Synthesis, hydrogen-1 NMR, and crystallographic studies of cationic complexes of MeHg(II) with ambidentate and polydentate ligands containing pyridyl and N-substituted imidazolyl donors and involving unusual coordination geometries. *Inorg. Chem.* **1981**, *20*, 2414-2422.

[23] Sommerfeld, N. S.; Gülzow, J.; Roller, A.; Cseh, K.; Jakupec, M. A.; Grohmann, A.; Galanski, M.; Keppler, B. K., Antiproliferative Copper(II) and Platinum(II) Complexes with Bidentate N,N-Donor Ligands. *Chem. Eur. J.* **2017**, *2017*, 3115-3124.

[24] Byers, P. K.; Canty, A. J., Synthetic routes to methylpalladium(II) and dimethylpalladium(II) chemistry and the synthesis of new nitrogen donor ligand systems. *Organometallics* **1990**, *9*, 210-220.

[25] Jones, M. R.; Fast, C. D.; Schley, N. D., Iridium-Catalyzed sp^3 C–H Borylation in Hydrocarbon Solvent Enabled by 2,2′-Dipyridylarylmethane Ligands. *J. Am. Chem. Soc.* **2020,** *142*, 6488-6492.

[26] Rudolph, M., Digital simulations on unequally spaced grids.: Part 2. Using the box method by discretisation on a transformed equally spaced grid. *J. Electroanal. Chem.* **2003**, *543*, 23-39.

[27] (a) Canty, A. J.; Chaichit, N.; Gatehouse, B. M.; George, E . E.; Hayhurst, G., Coordination chemistry of methylmercury(II). Synthesis, hydrogen-1 NMR, and crystallographic studies of cationic complexes of MeHg(II) with ambidentate and polydentate ligands containing pyridyl and N-substituted imidazolyl donors and involving unusual coordination geometries. *Inorg. Chem.*, **1981**, 20, 2414–2422. (b) Byers, P. K.; Canty, A. J., Synthetic routes to methylpalladium(II) and dimethylpalladium(II) chemistry and the synthesis of new nitrogen donor ligand systems. *Organometallics*, **1990**, 9, 210–220. (c) Mohr, F.; Binfield, S. A.; Fettinger, J. C.; Vedernikov, A. N., A Practical, Fast, and High-Yielding Aziridination Procedure Using Simple Cu(II) Complexes Containing N-Donor Pyridine-Based Ligands. *J. Org. Chem.,* **2005**, 70, 4833–4839.

[28] Vedernikov, N.; Miftakhov, R.; Borisoglebski, S. V.; Caulton, K. G.; Solomonov, B. N., Condensation of 2-Pyridylmethyllithium Nucleophiles and Pyridine Electrophiles as a Convenient Synthetic Route to Polydentate Chelating N-Donor Ligands. *Chem. Heterocycl. Compd.* **2002**, *38*, 406-416.

[29] Golden, J. H.; Facendola, J. W.; Sylvinson M. R, D.; Baez, C. Q.; Djurovich, P. I.; Thompson, M. E., Boron Dipyridylmethene (DIPYR) Dyes: Shedding Light on Pyridine-Based Chromophores. *J. Org. Chem.* **2017**, *82*, 7215-7222.

[30] Kumari, N.; Dey, N.; Jha, S.; Bhattacharya, S., Ratiometric, Reversible, and Parts per Billion Level Detection of Multiple Toxic Transition Metal Ions Using a Single Probe in Micellar Media. *ACS App. Mat. Interfaces* **2013**, *5*, 2438-2445.

[31] White, C.; Yates, A.; Maitlis, P. M., (η^5-Pentamethylcyclopentadienyl)Rhodium and -Iridium Compounds. *Inorg. Synth.* **1992**, 29, 228–234

[32] Mantell, M. A.; Kampf, J. W.; Sanford, M., Improved Synthesis of $[Cp^RRhCl_2]_2$ Complexes. *Organometallics* **2018**, *37*, 3240-3242.

[33] Nutton, A.; Bailey, P. M.; Maitlis, P. M., Pentamethylcyclopentadienyl-rhodium and -iridium complexes. Part 29. Syntheses and *X*-ray structure determinations of $[\{Rh(C_5Me_5)\}_2(OH)_3]OH{\cdot}11H_2O$ and $[\{lr(C_5Me_5)\}_2(OH)_3]O_2CMe{\cdot}14H_2O$ and related complexes. *J. Chem. Soc., Dalton Trans.* **1981**, 1997–2002.

[34] Dadci, L.; Elias, H.; Frey, U.; Hoernig, A.; Koelle, U.; Merbach, A. E.; Paulus, H.; Schneider, J. S., .pi.-Arene Aqua Complexes of Cobalt, Rhodium, Iridium, and Ruthenium: Preparation, Structure, and Kinetics of Water Exchange and Water Substitution. *Inorg. Chem.* **1995**, *34*, 306-315.

[35] Hammett, L. P., The Effect of Structure upon the Reactions of Organic Compounds. Benzene Derivatives. *J. Am. Chem. Soc.* **1937**, *59*, 96-103.

[36] (a) Ševčík, A., Oscillographic polarography with periodical triangular voltage. *Collect. Czech. Chem. Commun.* **1948**, *13*, 349-377 (b) Randles, J. E. B., A cathode ray polarograph. Part II.—The current-voltage curves. *Trans. Faraday Soc.* **1948**, *44*, 327-338.

[37] Ashford, D. L.; Gish, M. K.; Vannucci, A. K.; Brennaman, M. K.; Templeton, J. L.; Papanikolas, J. M.; Meyer, T. J., Molecular Chromophore–Catalyst Assemblies for Solar Fuel Applications. *Chem. Rev.* **2015**, *115*, 13006-13049.

[38] (a) Lewis, N. S.; Nocera, D. G., Powering the planet: Chemical challenges in solar energy utilization. *Proc. Nat. Acad. Sci. U.S.A.* **2006**, *103*, 15729-15735. (b) Young, K. J.; Martini, L. A.; Milot, R. L.; Snoeberger III, R. C.; Batista, V. S.; Schmuttenmaer, C. A.; Crabtree, R. H.; Brudvig, G. W., Light-driven water oxidation for solar fuels. *Coord. Chem. Rev.* **2012**, 256, 2503–2520.

[39] (a) Nichols, A. W.; Machan, C. W., Secondary-Sphere Effects in Molecular Electrocatalytic CO2 Reduction. *Frontiers in Chemistry* **2019**, 7. (b) Haviv, E.; Azaiza-Dabbah, D.; Carmieli, R.; Avram, L.; Martin, J. M. L.; Neumann, R., A Thiourea Tether in the Second Coordination Sphere as a Binding Site for CO_2 and a Proton Donor Promotes the Electrochemical Reduction of CO_2 to CO Catalyzed by a Rhenium Bipyridine-Type Complex. *J. Am. Chem. Soc.* **2018**, *140*, 12451-12456. (c) Rotundo, L.; Garino, C.; Priola, E.; Sassone, D.; Rao, H.; Ma, B.; Robert, M.; Fiedler, J.; Gobetto, R.; Nervi, C., Electrochemical and Photochemical Reduction of CO_2 Catalyzed by Re(I) Complexes Carrying Local Proton Sources. *Organometallics* **2019**, *38*, 1351-1360.

[40] Geiger, W. E., Organometallic Electrochemistry: Origins, Development, and Future. *Organometallics* **2007**, *26*, 5738-5765.

[41] Fulmer, G. R.; Miller, A. J. M.; Sherden, N. H.; Gottlieb, H. E.; Nudelman, A.; Stoltz, B. M.; Bercaw, J. E.; Goldberg, K. I., NMR Chemical Shifts of Trace Impurities: Common Laboratory Solvents, Organics, and Gases in Deuterated Solvents Relevant to the Organometallic Chemist. *Organometallics* **2010**, *29*, 2176-2179.

[42] (a) Harris, R. K.; Becker, E. D.; Cabral De Menezes, S. M.; Goodfellow, R.; Granger, P., NMR nomenclature. Nuclear spin properties and conventions for chemical shifts (IUPAC Recommendations 2001) *Pure Appl. Chem.* **2001**, *73*, 1795– 1818. (b) Harris, R. K.; Becker, E. D.; Cabral De Menezes, S. M.; Granger, P.; Hoffman, R. E.; Zilm, K. W., Further conventions for NMR shielding and chemical shifts (IUPAC Recommendations 2008). *Pure Appl. Chem.* **2008**, 80, 59–84.

For Table of Contents Only:

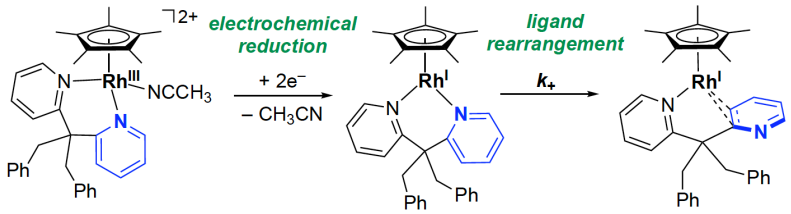

TOC Synopsis:

Chemical and electrochemical methods have been used to quantify the rate of a reduction-induced ligand rearrangement that occurs in a series of new [Cp*Rh] compounds bearing substituted di-pyridylmethane ligands. Simulations of cyclic voltammetry data have been used to extract the rate constants for several derivatives, revealing that the bulkier ligands "flip" more slowly.